

Supporting Information

**Visible responses under high pressure in crystals: phenolphthalein
and its analogues with adjustable ring-opening threshold pressures**

Xinyuan Deng,^a Hongwei Guo,^b Xiao Meng,^a Kai Wang,^b Bo Zou^{*b} and Yuguo Ma^{*a}

*a. Beijing National Laboratory for Molecular Sciences (BNLMS), Center for Soft Matter
Science and Engineering, Key Lab of Polymer Chemistry & Physics of Ministry of
Education, College of Chemistry, Peking University, Beijing 100871, China*

*b. State Key Laboratory of Superhard Materials, College of Physics, Jilin University,
Changchun 130012, China*

Table of Contents

<i>Experimental Section</i>	2
<i>UV Radiation Experiments</i>	4
<i>In situ UV-vis Absorption and Raman Spectra</i>	4
<i>Quantify the Relationship between Pressure and the Ring-opening Reaction</i>	9
<i>Crystal Data and Structure Refinement</i>	10
<i>References</i>	16

Experimental Section

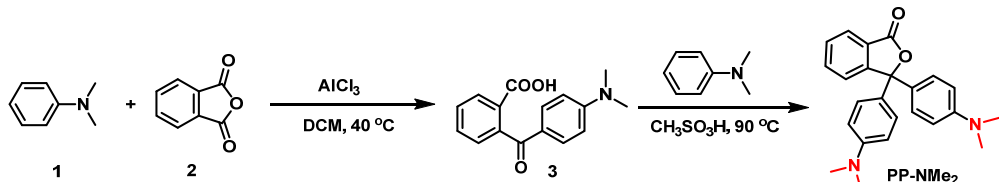
General Methods: Chemicals were purchased commercially and used without further purification unless otherwise noted. Tetrahydrofuran (THF) was freshly distilled from sodium under N₂ prior to use. Dichloromethane (DCM) was freshly distilled from calcium hydride under N₂ prior to use. PMMA was purchased from ourchem, and its M_w is 35,000 Da. ¹H NMR and ¹³C NMR spectra were recorded on a Bruker-400 (400 MHz) spectrometer using CDCl₃ as solvent. Chemical shifts are reported in parts per million (ppm). ¹H NMR chemical shifts were referenced versus TMS (0 ppm), while ¹³C NMR chemical shifts were referenced versus CDCl₃ (77.0 ppm). Mass spectra were recorded on a VG ZAB-HS mass spectrometer. Powder X-ray diffraction (PXRD) data was collected on a PHILIPS X’Pert Pro diffractometer with an X’celerator detector in the reflection mode, using monochromatized Cu K α radiation.

High pressure experiments were performed using symmetric diamond anvil cells (DACS) at room temperature. The culet diameter of the diamond anvils was 500 μ m. The crystal was placed in the holes (diameter: ca. 170 μ m) of a T301 steel gasket, which was pre-indented to a thickness of 50 μ m. The silicon oil was used as pressure transmitting medium (PTM). A small ruby chip was inserted into the sample compartment for *in situ* pressure calibration according to the R1 ruby fluorescence method. The *in situ* UV-vis absorption measurements under high pressure are performed on an Ocean Optics QE65000 Scientific-grade spectrometer. The photoluminescence measurements under high pressure were performed on a QE65000 Scientific-grade spectrometer in the reflection mode. High-pressure unpolarized Raman spectra were recorded using Acton SP2500i spectrometer (Princeton Instruments) equipped with the liquid nitrogen cooled CCD (PyLon: 100B). The 532 nm radiation from the diode pumped solid state (DPSS) laser was utilized to excite the sample and the output power was 10 mW. The 785 nm single mode laser was utilized to excite the sample and the output power was 50 mW.

Synthesis and Characterization:

PP was purchased from TCI company with >98% purity, and recrystallized in ethanol before use. **PP-NMe₂** was synthesized by optimizing the reaction conditions in the literature¹. **PP-H** was synthesized according to the literature². The single crystal of **PP-NMe₂** was obtained from dichloromethane/petroleum ether. The single crystal of **PP-H** was obtained from ethyl acetate/petroleum ether.

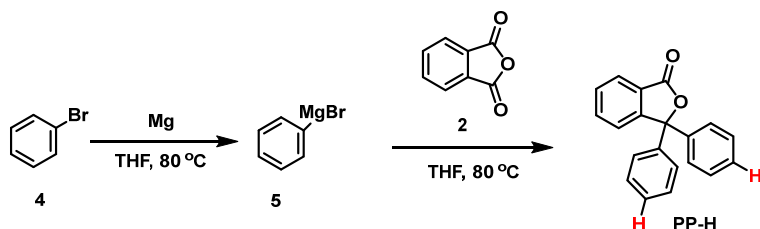
3,3-bis(4-(dimethylamino)phenyl)isobenzofuran-1(3H)-one (**PP-NMe₂**)



To a stirred solution of phthalic anhydride **2** (3.26 g, 22 mmol) and aluminum chloride

(8.80 g, 66 mmol) in 50 mL anhydrous dichloromethane, *N,N*-dimethylaniline (2.5 mL, 22 mmol) was added slowly at room temperature (rt). Then the reaction was heated to 40 °C for 3 h. The reaction was cooled to rt, and poured into ice water. Sodium hydroxide was added to adjust the pH around 2-3. Some precipitate came out in the solution and was filtered out. The pH of the filtrate was adjusted to 3-4, and the precipitate was filtered out. The filter residue **3** was dried. To a solution of **3** (2.9 g, 11 mmol) in 10 mL methanesulfonic acid, *N,N*-dimethylaniline (2.7 mL, 22 mmol) was added at rt. The mixture was heated at 90 °C for 12 h. The reaction was cooled to rt, and ice water was added. The resulting mixture was extracted with dichloromethane (3 × 20 mL). The combined organic layers were then extracted with brine. Then it was dried over MgSO₄ and filtered. The solvent was removed under reduced pressure. The resulting residue was purified by column chromatography using dichloromethane/petroleum ether as eluent. Compound **PP-NMe₂** was obtained as white crystalline solid (1.6 g, 20%). ¹H NMR (400 MHz, CDCl₃): δ 7.90 (d, *J* = 7.4 Hz, 1H), 7.64 (t, *J* = 7.5 Hz, 1H), 7.49 (t, *J* = 7.5 Hz, 2H), 7.18 (d, *J* = 8.8 Hz, 4H), 6.63 (d, *J* = 8.8 Hz, 4H), 2.93 (s, 12H). ¹³C NMR (100 MHz, CDCl₃): δ 170.5, 153.5, 150.3, 133.7, 128.7, 128.6, 128.2, 125.8, 125.7, 123.9, 92.7, 40.4. HRMS (ESI) m/z: [M + H]⁺ calcd for C₂₄H₂₅N₂O₂, 373.1912; found, 373.1911.

3,3-diphenylisobenzofuran-1(3H)-one (**PP-H**)



The magnesium ribbon was burnished and cut into small pieces. Mg (0.10 g, 4.2 mmol) and bromobenzene **4** (0.40 mL, 3.8 mmol) were dissolved in 10 mL anhydrous THF, and stirred at 80 °C for 2 h under N₂ atmosphere. Then the mixture was cooled to rt, and added to a THF solution of phthalic anhydride **2** (0.28 g, 1.9 mmol) slowly under N₂ atmosphere at 0 °C. The reaction was heated at 80 °C for 12 h. The reaction was quenched by aqueous solution of HCl (1.0 N) and extracted with ethyl acetate (3 × 20 mL). The combined organic layer was dried over MgSO₄ and filtered. The solvent was evaporated under reduced pressure. The resulting residue was purified by column chromatography using dichloromethane/petroleum ether as an eluent. Compound **PP-H** was obtained as a white crystalline solid (0.21 g, 40%). ¹H NMR (400 MHz, CDCl₃): δ 7.95 (d, *J* = 7.6 Hz, 1H), 7.74-7.67 (m, 1H), 7.64-7.50 (m, 2H), 7.34 (m, 10H). ¹³C NMR (100 MHz, CDCl₃): δ 170.5, 153.5, 150.3, 133.7, 128.7, 128.6, 128.2, 125.8, 125.7, 123.9, 92.7, 40.4. HRMS (ESI) m/z: [M + H]⁺ calcd for C₂₀H₁₅O₂, 287.1074; found, 287.1067.

UV Radiation Experiments

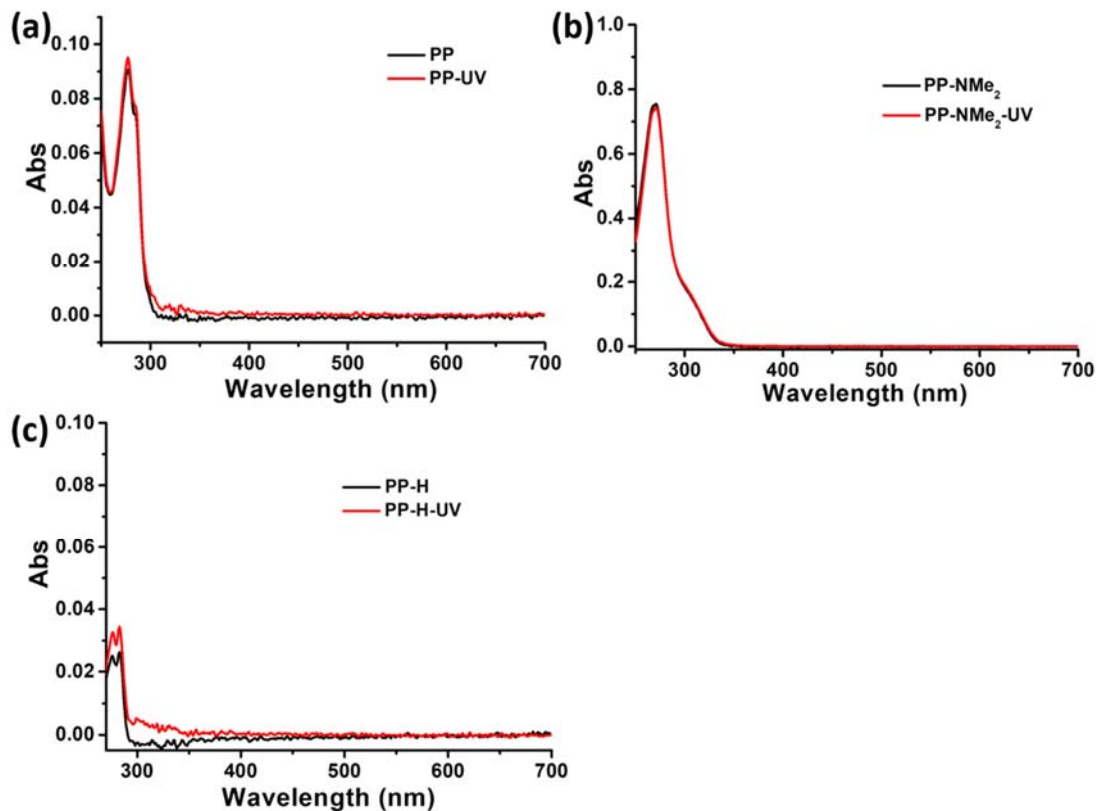


Figure S1. UV-vis absorption spectra before and after UV irradiation with Hg lamp at 365 nm (500 W) for 1 h for (a) PP, (b) PP-NMe₂, and (c) PP-H.

In situ UV-vis Absorption and Raman Spectra

1) In situ UV-vis Absorption Spectra for PP

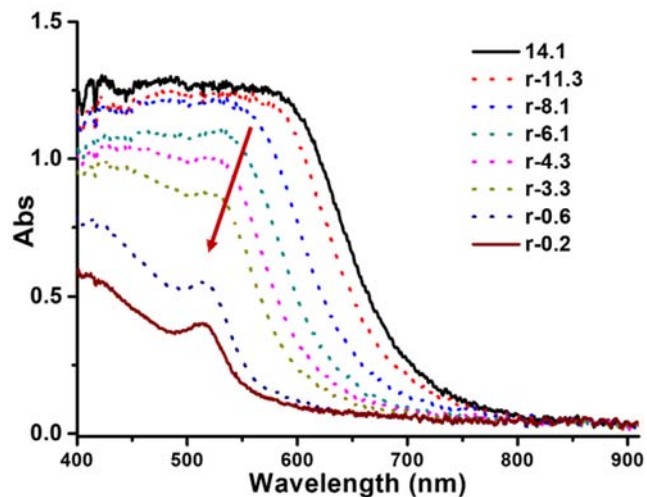


Figure S2. In situ UV-vis absorption spectra of PP under high pressure during decompression process.

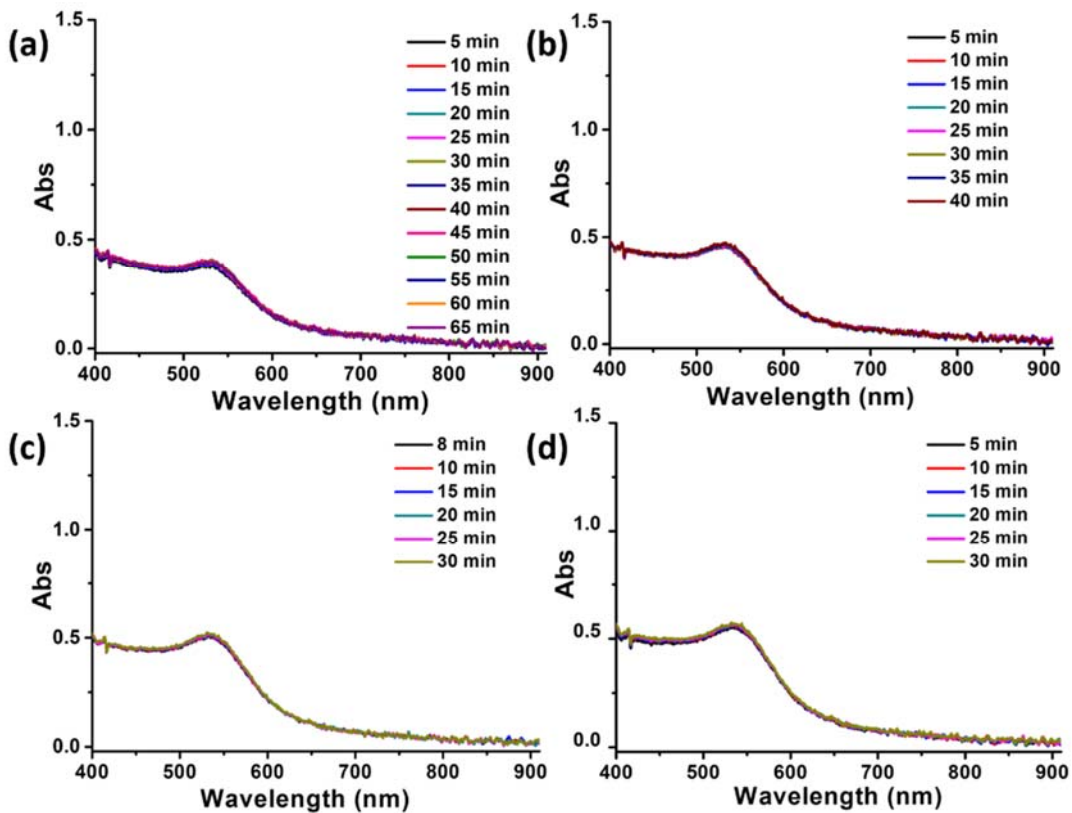


Figure S3. *In situ* UV-vis absorption spectra of PP over different time under the pressure of (a) 8.5 GPa; (b) 9.2 GPa; (c) 9.6 GPa; (d) 10.0 GPa.

2) *In situ* UV-vis Absorption Spectra for PP-NMe₂

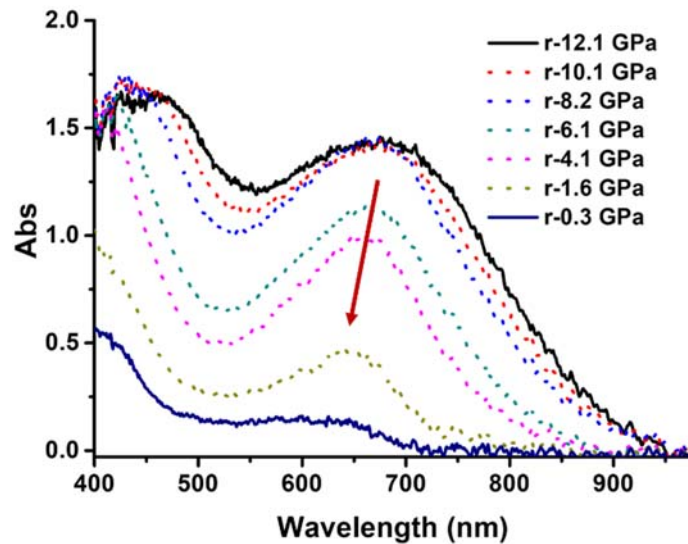


Figure S4. *In situ* UV-vis absorption spectra of PP-NMe₂ under high pressure during decompression process.

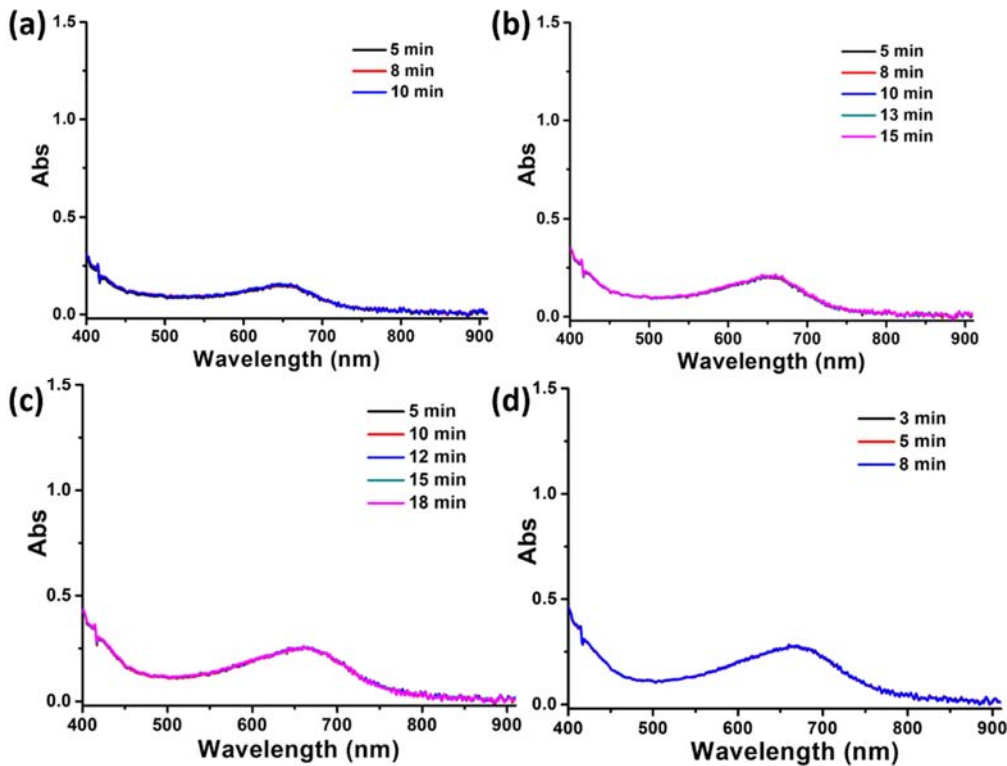


Figure S5. UV-vis absorption spectra *in situ* of **PP-NMe₂** over different time under the pressure of (a) 5.2 GPa; (b) 6.0 GPa; (c) 8.9 GPa; (d) 9.2 GPa.

3) *In situ* Raman Spectra of **PP-NMe₂**

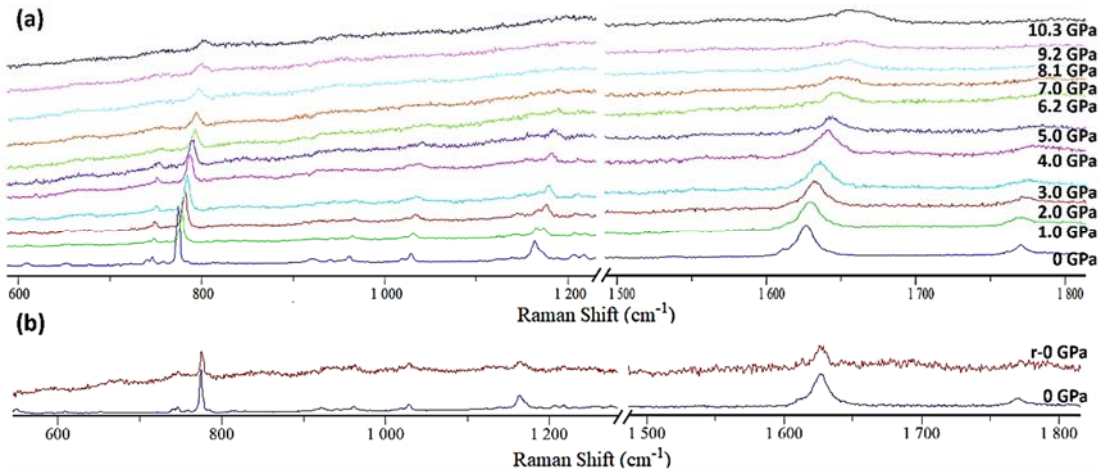


Figure S6. (a): *in situ* Raman spectroscopy ($\lambda_{\text{ex}} = 532 \text{ nm}$) of **PP-NMe₂** under compression process in the range of 0-10.3 GPa; (b): *in situ* Raman spectroscopy of **PP-NMe₂** before and after pressure treatment.

Relative more intense Raman peaks were chosen to demonstrate the changes in the wave numbers ranging of 100-3600 cm^{-1} . The excitation wavelengths only influence the range of Raman spectra, longer excitation wavelength (785 nm compared with 532 nm) could reduce the interference of fluorescence.

4) *In situ* Raman Spectra of PP

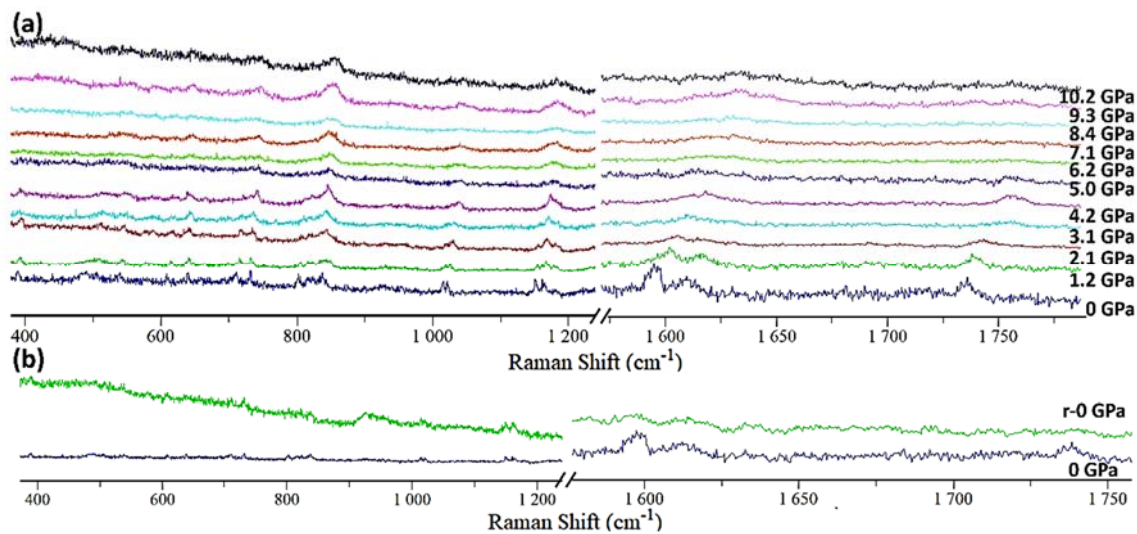


Figure S7. (a): *in situ* Raman spectroscopy ($\lambda_{\text{ex}} = 785 \text{ nm}$) of PP under compression process in the range of 0-10.2 GPa; (b): *in situ* Raman spectroscopy of PP before and after pressure treatment.

5) *In situ* Raman Spectra of PP-H

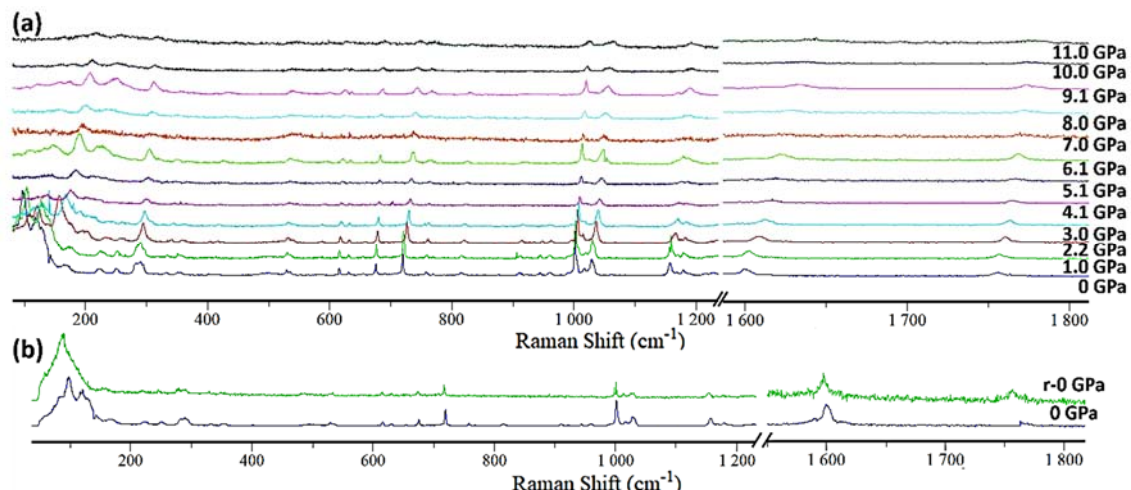


Figure S8. (a): *in situ* Raman spectroscopy ($\lambda_{\text{ex}} = 785 \text{ nm}$) of PP-H under compression process in the range of 0-11.0 GPa; (b): *in situ* Raman spectroscopy of PP-H before and after pressure treatment.

6) *In situ* UV-vis Absorption Spectra for PP-H

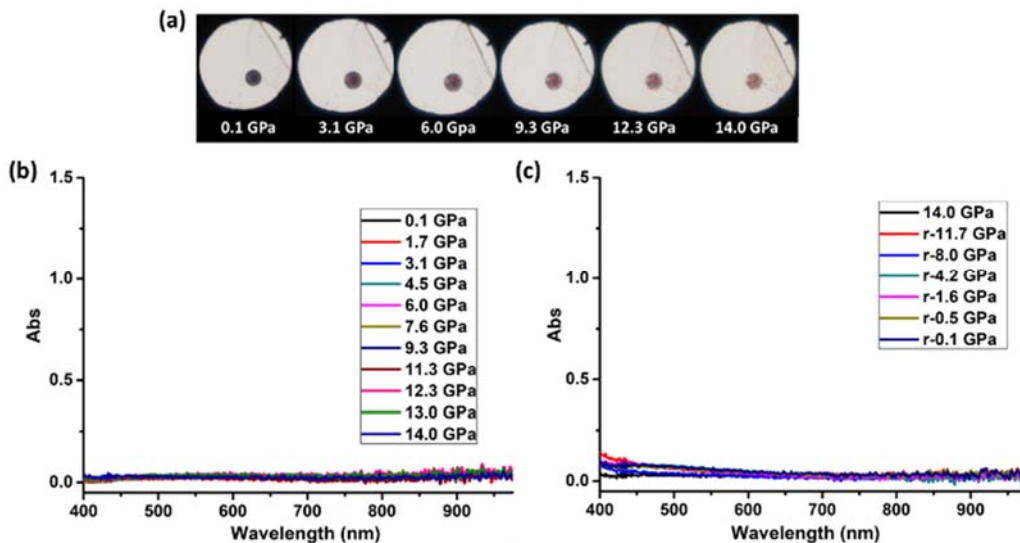


Figure S9. (a) Real optical images of **PP-H** crystal in the compression process; (b) *in situ* UV-vis absorption spectra of **PP-H** under compression in the range of 0-14.0 GPa; (c) *in situ* UV-vis absorption spectra of **PP-H** under high pressure during the decompression process.

7) *In situ* UV-vis Absorption Spectra for **PP-NMe₂** dispersed in PMMA film

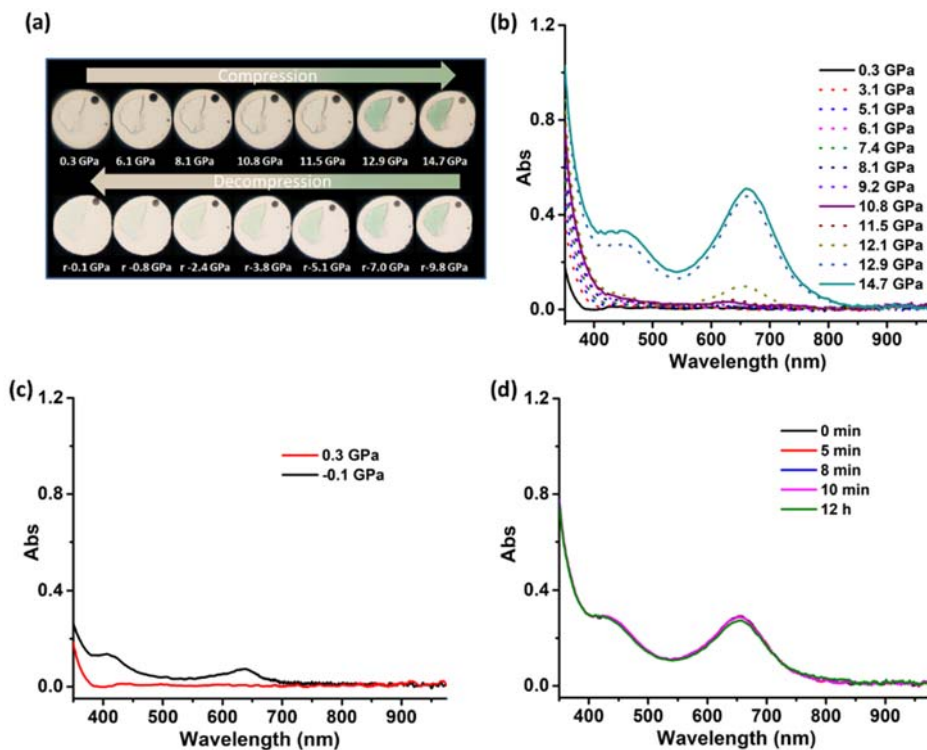


Figure S10. **PP-NMe₂** (5 wt%) PMMA film (a) Real optical images under different pressures; (b) *in situ* UV-vis absorption spectra under compression in the range of 0-13.2 GPa; (c) The comparison of UV-vis absorption spectra before (0.3 GPa) and after (r-0.1 GPa) the pressure treatment; (d) *in situ* UV-vis spectra over different time under high pressure of r-9.8 GPa.

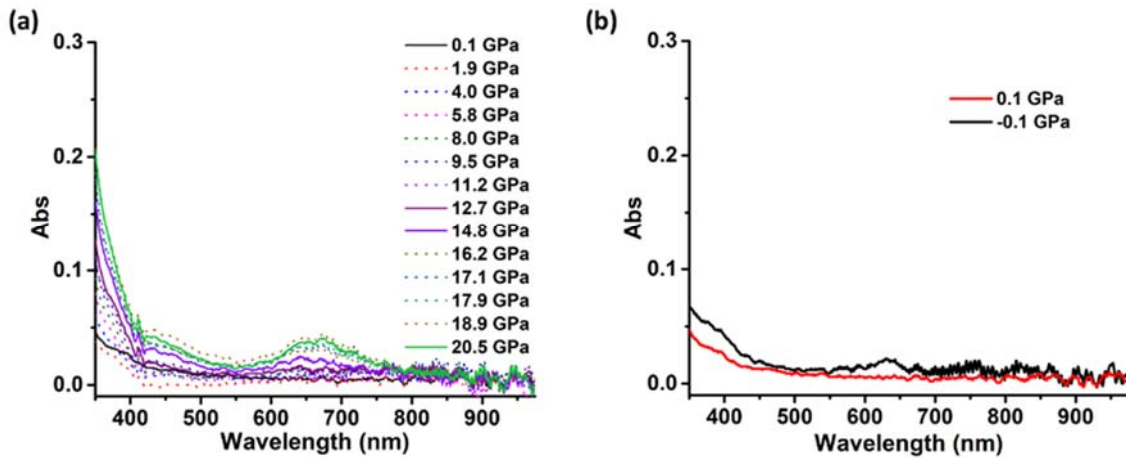


Figure S11. PP-NMe₂ (1 wt%) PMMA film (a) *In situ* UV-vis absorption spectra under compression in the range of 0–20.5 GPa; (b) The comparison of UV-vis absorption spectra before (0.1 GPa) and after (r-0.1 GPa) the pressure treatment.

Quantify the Relationship between Pressure and the Ring-opening Reaction

- 1) Equilibrium constant K of the ring-opening reaction could be quantified from the fraction of **r-PP** (ring-opening **PP**) as follows:

$$K = \frac{n(r-PP)}{n-n(r-PP)}$$

The n refers to the amount of **PP** (including ring-closed and -opened **PP**), and $n(r-PP)$ means the amount of ring-opening **PP**. For a specific experiment, the n could be regarded as a constant. At the beginning of the ring-opening reaction, the conversion in crystal is low, so the $n-n(r-PP)$ is approximately equal to n , in order to get qualitative information and get an approximate working curve. Then $1/(n-n(r-PP))$ is regarded as a constant to simplify the formula. (Higher conversion as the increased pressure is one of the reasons to make correlation of $\ln A(r-PP)$ with pressure (p) deviate from the straight line.)

Furthermore, $n(r-PP)$ was proportional to absorbance of the characteristic absorption peak of **r-PP**, then $\ln K$ is approximated to be proportional to the natural logarithm of **r-PP** form:

$$\ln K \propto \ln A(r-PP) + C \quad (1)$$

- 2) The effect of pressure on chemical equilibrium could be described by the well-known relationship between pressure (p) and Gibbs' enthalpy of reaction³:

$$\Delta V = \left(-\frac{\partial \Delta G}{\partial p} \right)_T = \left(-\frac{\partial \ln K}{\partial p} \right)_T RT \quad (2)$$

Where ΔV is the change of the volume in the ring-opening reaction.

According to (1) and (2), we can derive the following relationship:

$$\frac{\partial \ln A(r-PP)}{\partial p} \propto \frac{\partial \ln K}{\partial p} = -\frac{\Delta V}{RT}$$

From the correlation, it showed that positive slope indicated a negative value for the volume of reaction, the same as spiropyran isomerization under high pressure⁴. The correlation wavelength was chosen around the ring-opening wavelength.

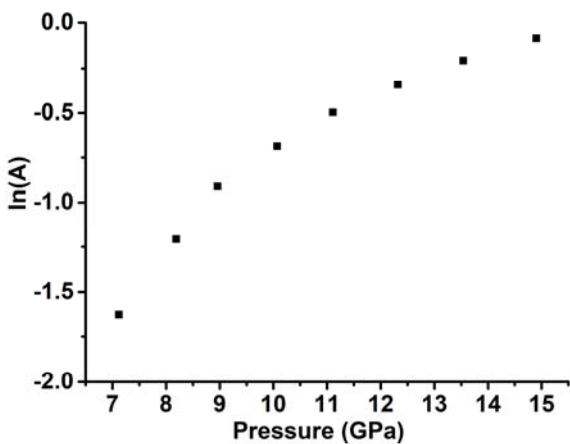


Figure S12. Correlation of $\ln A(\text{PP})$ at 533 nm with pressure (P) in a pressure range of 7.0-14.0 GPa.

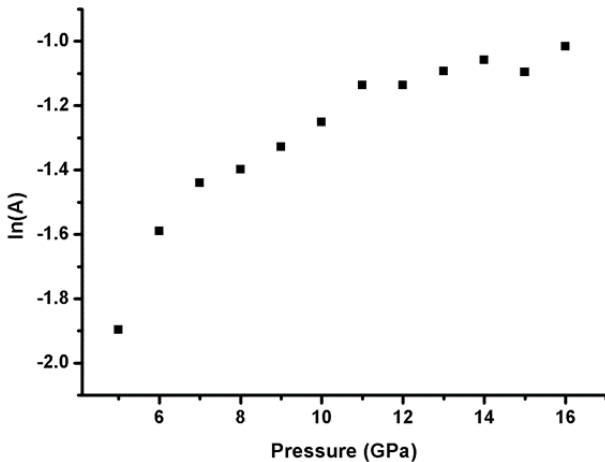
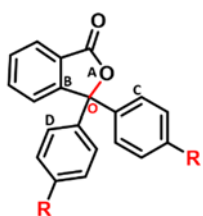


Figure S13. Correlation of $\ln A(\text{PP-NMe}_2)$ at 653 nm with pressure (P) in a limited pressure range of 5.0 -16.0 GPa.

Crystal Data and Structure Refinement

Table S1. The comparison of angles [deg] on the sp^3 carbon (labeled as O) for **PP**, **PP-NMe₂**, **PP-H**.



	PP	PP-NMe₂	PP-H
Angle AOB	102.35	101.56	102.31
Angle AOC	107.03	107.45	106.56
Angle AOD	107.61	107.84	107.85
Angle COD	114.24	115.02	112.14
Angle BOD	109.11	113.10	110.90
Angle BOC	115.50	117.78	116.20

Table S2-1. Crystal data and structure refinement for **PP-NMe₂**.

Identification code	PP-NMe₂	
Empirical formula	C ₂₄ H ₂₄ N ₂ O ₂	
Formula weight	372.45	
Temperature	180.01(10) K	
Wavelength	0.71073 Å	
Crystal system, Space group	Monoclinic, P2 ₁ /n	
Unit cell dimensions	a = 7.8706(16) Å	α= 90 deg.
	b = 21.886(5) Å	β= 97.560(19)deg.
	c = 11.121(3) Å	γ= 90 deg.
Volume	1898.9(8) Å ³	
Z, Density (calculated)	4, 1.303 Mg/m ³	
Absorption coefficient	0.083 mm ⁻¹	
F(000)	792.0	
Crystal size	0.1 × 0.1 × 0.05 mm ³	
Theta range for data collection	6.414 to 52.02 deg.	
Index ranges	-9<=h<=9, -20<=k<=26, -7<=l<=13	
Reflections collected	7099	
Independent reflections	3689 [R _{int} = 0.0587]	
Absorption correction	Semi-empirical from equivalents	
Refinement method	Full-matrix least-squares on F ²	
Data / restraints / parameters	3689 / 0 / 257	
Goodness-of-fit on F ²	1.046	
Final R indexes [I>=2sigma(I)]	R1 = 0.0806, wR2 = 0.1949	
R indexes [all data]	R1 = 0.1161, wR2 = 0.2352	
Largest diff. peak and hole	0.45 and -0.32 e.Å ⁻³	

Table S2-2. Atomic coordinates ($\times 10^4$) and equivalent isotropic displacement parameters ($\text{\AA}^2 \times 10^3$) for **PP-NMe₂**. U(eq) is defined as one third of the trace of the orthogonalized U^{ij} tensor.

	x	y	z	U(eq)
C1	1895(4)	893.0(13)	1221(3)	37.0(7)
C2	2095(3)	1696.4(12)	2627(2)	32.6(7)
C3	239(3)	1535.5(12)	2207(2)	32.3(7)
C4	-1245(4)	1787.6(14)	2542(3)	40.3(7)
C5	-2793(4)	1529.3(14)	2058(3)	44.7(8)
C6	-2884(4)	1037.8(14)	1278(3)	46.8(8)
C7	-1395(4)	789.1(14)	937(3)	42.5(8)
C8	140(4)	1052.7(12)	1417(2)	33.5(7)
C9	2547(3)	2347.5(12)	2314(2)	32.2(6)
C10	1999(4)	2563.1(13)	1150(3)	37.9(7)
C11	2359(4)	3145.5(13)	809(3)	39.4(7)
C12	3234(3)	3558.9(12)	1613(2)	34.8(7)
C13	3810(4)	3338.1(14)	2777(3)	40.1(7)
C14	3479(4)	2743.2(13)	3094(3)	39.3(7)
C15	3452(4)	4315.2(14)	40(3)	48.8(8)
C16	4467(4)	4561.9(14)	2142(3)	49.3(8)
C17	2595(3)	1518.3(12)	3947(2)	32.7(7)
C18	3506(3)	994.3(13)	4288(3)	37.6(7)
C19	3903(4)	828.7(13)	5491(3)	41.0(7)
C20	3388(4)	1188.4(13)	6413(3)	36.8(7)
C21	2437(4)	1708.9(13)	6061(3)	39.8(7)
C22	2034(4)	1864.1(13)	4857(3)	37.0(7)
C23	4743(4)	484.9(16)	7950(3)	55.2(9)
C24	3869(5)	1499.2(16)	8524(3)	55.1(9)
N1	3485(3)	4157.3(11)	1310(2)	42.7(7)
N2	3748(3)	1026.0(11)	7618(2)	44.4(7)
O1	2999(2)	1280.1(8)	1884.4(17)	35.9(5)
O2	2404(3)	510.9(10)	587(2)	49.9(6)

Table S2-3. Bond lengths [Å] and angles [deg] for **PP-NMe₂**

C1-C8	1.468(4)	O1-C2-C17	107.4(2)
C1-O1	1.360(3)	C4-C3-C2	129.5(3)
C1-O2	1.196(3)	C8-C3-C2	110.4(2)
C2-C3	1.515(4)	C8-C3-C4	120.1(2)
C2-C9	1.520(4)	C3-C4-C5	117.5(3)
C2-C17	1.520(4)	C6-C5-C4	122.2(3)
C2-O1	1.474(3)	C5-C6-C7	120.1(3)
C3-C4	1.386(4)	C8-C7-C6	117.2(3)
C3-C8	1.370(4)	C3-C8-C1	107.7(2)
C4-C5	1.386(4)	C3-C8-C7	122.9(3)
C5-C6	1.378(5)	C7-C8-C1	129.4(3)
C6-C7	1.390(4)	C10-C9-C2	118.5(2)
C7-C8	1.381(4)	C14-C9-C2	124.8(2)
C9-C10	1.392(4)	C14-C9-C10	116.7(2)
C9-C14	1.369(4)	C11-C10-C9	121.5(3)
C10-C11	1.370(4)	C10-C11-C12	122.1(3)
C11-C12	1.390(4)	C11-C12-C13	116.3(3)
C12-C13	1.400(4)	N1-C12-C11	122.6(3)
C12-N1	1.373(4)	N1-C12-C13	121.1(3)
C13-C14	1.382(4)	C14-C13-C12	120.8(3)
C15-N1	1.451(4)	C9-C14-C13	122.5(3)
C16-N1	1.432(4)	C18-C17-C2	122.6(2)
C17-C18	1.379(4)	C18-C17-C22	117.3(3)
C17-C22	1.381(4)	C22-C17-C2	120.0(2)
C18-C19	1.382(4)	C17-C18-C19	121.8(3)
C19-C20	1.394(4)	C18-C19-C20	120.9(3)
C20-C21	1.391(4)	C21-C20-C19	116.9(3)
C20-N2	1.379(4)	N2-C20-C19	121.8(3)
C21-C22	1.377(4)	N2-C20-C21	121.2(3)
C23-N2	1.441(4)	C22-C21-C20	121.5(3)
C24-N2	1.439(4)	C21-C22-C17	121.5(3)
O1-C1-C8	108.5(2)	C12-N1-C15	118.8(2)
O2-C1-C8	130.4(3)	C12-N1-C16	120.9(3)
O2-C1-O1	121.0(3)	C16-N1-C15	114.9(2)
C3-C2-C9	113.1(2)	C20-N2-C23	119.7(3)
C3-C2-C17	110.8(2)	C20-N2-C24	118.7(2)
C17-C2-C9	115.0(2)	C24-N2-C23	115.4(3)
O1-C2-C3	101.6(2)	C1-O1-C2	111.6(2)
O1-C2-C9	107.8(2)		

Table S3-1. Crystal data and structure refinement for **PP-H**.

Identification code	PP-H		
Empirical formula	$C_{20}H_{14}O_2$		
Formula weight	286.31		
Temperature	180.01(10) K		
Wavelength	0.71073 Å		
Crystal system, Space group	Monoclinic, $P21/n$		
Unit cell dimensions	$a = 8.4905(6)$ Å	$\alpha = 90$ deg.	
	$b = 17.1536(11)$ Å	$\beta = 100.649(6)$ deg.	
	$c = 10.3607(6)$ Å	$\gamma = 90$ deg.	
Volume	1482.97(17) Å ³		
Z, Density (calculated)	4, 1.282 Mg/m ³		
Absorption coefficient	0.082 mm ⁻¹		
F(000)	600.0		
Crystal size	0.1 × 0.1 × 0.05 mm ³		
Theta range for data collection	6.812 to 52.014°		
Index ranges	-10≤h≤6, -21≤k≤19, -10≤l≤12		
Reflections collected	5230		
Independent reflections	2881 [R _{int} = 0.0278, R _{sigma} = 0.0469]		
Absorption correction	Semi-empirical from equivalents		
Refinement method	Full-matrix least-squares on F ²		
Data / restraints / parameters	2881 / 0 / 199		
Goodness-of-fit on F ²	1.039		
Final R indexes [I>=2sigma(I)]	R1 = 0.0462, wR2 = 0.0979		
R indexes [all data]	R1 = 0.0739, wR2 = 0.1155		
Largest diff. peak and hole	0.21 and -0.19 e.Å ⁻³		

Table S3-2. Atomic coordinates ($\times 10^4$) and equivalent isotropic displacement parameters ($\text{\AA}^2 \times 10^3$) for PP-H. U(eq) is defined as one third of the trace of the orthogonalized U^{ij} tensor.

	x	y	z	U(eq)
O1	9921.9(14)	6804.7(7)	4996.5(11)	31.1(3)
O2	9358.8(17)	6239.3(9)	6800.4(13)	50.1(4)
C2	9073(2)	7076.7(10)	3706.0(15)	26.6(4)
C15	9361(2)	7950.2(10)	3662.2(15)	27.4(4)
C3	7362(2)	6823.7(10)	3713.4(16)	27.0(4)
C9	9758.5(19)	6642.1(10)	2655.8(16)	27.1(4)
C1	8888(2)	6476.3(11)	5704.1(17)	33.4(4)
C8	7285(2)	6476.3(10)	4896.9(16)	29.9(4)
C4	5997(2)	6873.2(11)	2746.6(17)	32.7(4)
C20	8176(2)	8474.8(11)	3148.0(17)	36.3(5)
C16	10909(2)	8223.6(11)	4108.5(17)	35.2(5)
C14	9840(2)	7000.7(11)	1475.7(17)	33.9(4)
C18	10063(3)	9527.5(12)	3546.8(19)	44.5(5)
C11	10829(2)	5477.2(11)	1864.6(18)	39.1(5)
C10	10241(2)	5874.5(11)	2829.3(17)	33.6(4)
C12	10923(2)	5842.5(12)	696.0(18)	38.4(5)
C19	8538(3)	9262.2(12)	3083.1(19)	44.2(5)
C7	5876(2)	6175.9(12)	5182.9(19)	40.7(5)
C13	10415(2)	6598.1(12)	499.4(18)	38.6(5)
C6	4516(2)	6238.6(13)	4232(2)	45.6(5)
C17	11247(3)	9009.7(12)	4062.3(19)	43.6(5)
C5	4577(2)	6582.4(12)	3033.9(19)	41.0(5)

Table S3-3. Bond lengths [Å] and angles [deg] for PP-H

O1-C2	1.4726(19)	C3-C2-C9	110.90(14)
O1-C1	1.365(2)	C20-C15-C2	122.96(15)
O2-C1	1.203(2)	C20-C15-C16	118.99(17)
C2-C15	1.520(2)	C16-C15-C2	117.99(16)
C2-C3	1.518(2)	C8-C3-C2	109.37(14)
C2-C9	1.521(2)	C8-C3-C4	119.95(16)
C15-C20	1.381(2)	C4-C3-C2	130.65(15)
C15-C16	1.392(2)	C14-C9-C2	120.21(16)
C3-C8	1.376(2)	C10-C9-C2	121.19(15)
C3-C4	1.387(2)	C10-C9-C14	118.53(16)
C9-C14	1.382(2)	O1-C1-C8	108.44(14)
C9-C10	1.381(3)	O2-C1-O1	120.83(17)
C1-C8	1.461(3)	O2-C1-C8	130.72(17)
C8-C7	1.383(3)	C3-C8-C1	108.51(15)
C4-C5	1.387(3)	C3-C8-C7	122.53(17)
C20-C19	1.390(3)	C7-C8-C1	128.95(16)
C16-C17	1.381(3)	C5-C4-C3	117.79(17)
C14-C13	1.386(3)	C15-C20-C19	119.98(18)
C18-C19	1.372(3)	C17-C16-C15	120.45(18)
C18-C17	1.373(3)	C9-C14-C13	120.38(18)
C11-C10	1.377(3)	C19-C18-C17	119.80(19)
C11-C12	1.379(3)	C10-C11-C12	120.00(18)
C12-C13	1.369(3)	C11-C10-C9	121.06(17)
C7-C6	1.377(3)	C13-C12-C11	119.53(17)
C6-C5	1.384(3)	C18-C19-C20	120.6(2)
C1-O1-C2	111.29(13)	C6-C7-C8	117.47(18)
O1-C2-C15	106.56(13)	C12-C13-C14	120.46(17)
O1-C2-C3	102.32(13)	C7-C6-C5	120.65(19)
O1-C2-C9	107.84(13)	C18-C17-C16	120.21(19)
C15-C2-C9	112.14(14)	C6-C5-C4	121.60(18)
C3-C2-C15	116.19(14)		

References

- (1) T. Bizjak, J. Karpiuk, S. Lochbrunner and E. Riedle, *J. Phys. Chem. A*, 2004, **108**, 10763-10769.
- (2) C. B. DeZutter, J. H. Horner and M. Newcomb, *J. Phys. Chem. A*, 2008, **112**, 1891-1896.
- (3) R. Van Eldik and F.-G. Klärner, High Pressure Chemistry: Synthetic, Mechanistic, and Supercritical Applications, John Wiley & Sons, 2008.
- (4) X. Meng, G. Qi, C. Zhang, K. Wang, B. Zou and Y. Ma, *Chem. Commun.*, 2015, **51**, 9320-9323.